

Machine learning optimization of Majorana hybrid nanowires

Matthias Thamm and Bernd Rosenow

Institut für Theoretische Physik, Universität Leipzig, Brüderstrasse 16, 04103 Leipzig, Germany

(Dated: August 10, 2022)

As the complexity of quantum systems such as quantum bit arrays increases, efforts to automate expensive tuning are increasingly worthwhile. We investigate machine learning based tuning of gate arrays using the CMA-ES algorithm for the case study of Majorana wires with strong disorder. We find that the algorithm is able to efficiently improve the topological signatures, learn intrinsic disorder profiles, and completely eliminate disorder effects. For example, with only 20 gates, it is possible to fully recover Majorana zero modes destroyed by disorder by optimizing gate voltages.

Introduction: In recent years, increasingly complex quantum devices have been proposed and implemented [1–5], requiring more personnel-intensive tuning. Therefore, it is becoming profitable, and in some cases even necessary, to automate the tuning process [6–8], and machine learning approaches have been found to be very flexible and robust for this purpose [5, 7–12]. Especially for the implementation of large scale quantum computation [13–16], efficient tuning of parameters and gates is crucial and numerous automations in quantum dot based qubits have been proposed [6–8, 10, 11, 17–23].

A popular platform for scalable qubit architectures is based on Majorana zero modes (MZMs) in topological superconductors [1, 4, 24–29], whose advantages are the non-local storage of quantum information and its manipulation via anyonic braiding [24–27, 30]. MZMs have been proposed to exist in semiconductor-superconductor heterostructures [24, 31–34] and many of their predicted signatures have been observed, such as zero-bias conductance peaks [35–38], the fractional Josephson effect [39], and the suppression of even-odd splitting difference of conductance resonances in Coulomb blockade [40]. For a clean wire, it has been theoretically demonstrated that a harmonic potential profile [41] and specially chosen magnetic field textures [41–44] can make MZMs more robust, and the geometry of Majorana Josephson junctions has been optimized to increase the size of the topological gap [45]. Nevertheless, disorder remains a crucial problem [46–49] in such systems, as it can mimic MZM signatures even in the topologically trivial region [46, 48, 50–53], or destroy the topological phase altogether [54].

In this letter, we present a case study of automatic tuning of a gate array in proximity to a strongly disordered Majorana wire using the CMA-ES [55, 56] algorithm. CMA-ES is a machine learning algorithm that does not need system specific information to operate, and is widely applicable for high dimensional optimization problems [57–61]. A crucial requirement is to find a good metric such that desired properties of the physical system are indeed improved during optimization. For example, signatures of MZMs can be mimicked by topologically trivial Andreev bound states (ABSs) [53, 62–78], which one would like to avoid. We therefore use the amplitude of coherent transmission [79–82] through a Coulomb-blocked

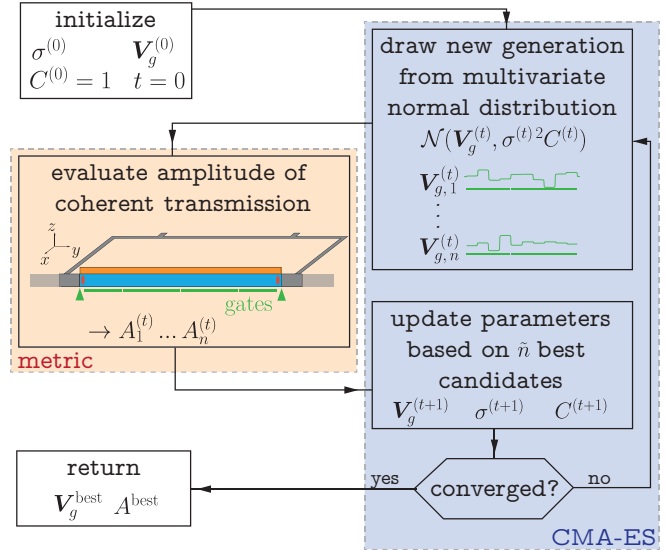


Figure 1. Schematic diagram of the Covariance Matrix Adaptation Evolution Strategy (CMA-ES) algorithm [55, 56] used to learn an optimal gate voltage configuration that maximizes the amplitude A of coherent transmission through a Majorana hybrid wire embedded into one arm of an Aharonov-Bohm interferometer. Initially, one sets a step size $\sigma^{(0)}$, a covariance matrix $C^{(0)}$, and starting gate voltages $\mathbf{V}_g^{(0)}$. In each iteration t , n gate voltage configurations are drawn from a multivariate normal distribution with mean $\mathbf{V}_g^{(t)}$ and covariance $C^{(t)}$. Based on the amplitudes A_i for the proposed gate voltage configurations $\mathbf{V}_{g,i}^{(t)}$, the new mean value $\mathbf{V}_g^{(t+1)}$ is determined, and step size $\sigma^{(t+1)}$ and covariance $C^{(t+1)}$ are updated.

Majorana wire as a metric, which can be measured by placing the wire in an arm of an electron interferometer [81] and allows to distinguish MZMs from ABSs [80, 82]. We find that as little as a few 100 to some 1000 amplitude measurements are sufficient to tune the gate array, such that (i) both the localization of the MZMs and the transmission amplitude are significantly improved, and (ii) strong potential disorder is compensated.

Setup: A schematic of the Majorana hybrid wire embedded in one arm of an Aharonov-Bohm interferometer and a flow diagram of the CMA-ES algorithm are shown in Fig. 1. Our goal is to find voltages V_j of N_g gates

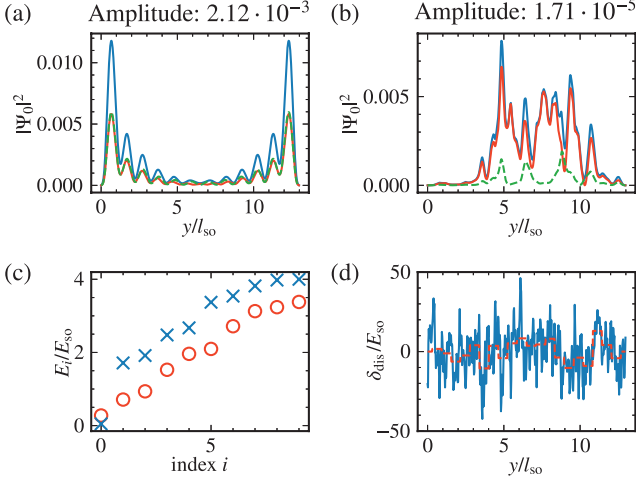


Figure 2. Reference results for deactivated gates: wave function $|\Psi_0|^2$ of the lowest level (blue), decomposed into hole wave function $|\mathbf{v}_0|^2$ (orange) and electron wave function $|\mathbf{u}_0|^2$ (green) for the case (a) without disorder, (b) with disorder strength $\sigma_{\text{dis}} = 50 E_{\text{so}}$ and correlation length $\lambda_{\text{dis}} = 0.052 l_{\text{so}}$. (c) Energies of the lowest ten Bogoliubov levels for the case without disorder (blue crosses) and with disorder (red circles). (d) Disorder potential along the wire (blue) and average of the disorder over gate regions (dashed, red).

such that the localization of MZMs inside the wires as well as their tunnel coupling to the connecting wires are optimized. For optimization purposes we Fourier expand the gate voltages as

$$V_j = \frac{b_0}{2} + \sum_{k=1}^{\lfloor \frac{N_g-1}{2} \rfloor} a_k \sin\left(\frac{2\pi}{N_g} k j\right) + \sum_{k=1}^{\lfloor \frac{N_g}{2} \rfloor} b_k \cos\left(\frac{2\pi}{N_g} k j\right). \quad (1)$$

Optimization of Fourier components has the advantage that by choosing $b_0 = 0$ and optimizing the remaining $N_g - 1$ components, the gate voltage is zero on average, whereas direct optimization of all the V_j and then manually removing the average according to $V_j \rightarrow V_j - \langle V_j \rangle$ negatively affects the robustness of the algorithm.

To obtain the spatial potential profile $V_g(y)$ acting on the hybrid wire, we assume that the wire is located at a distance z_0 from the gates, such that the potential profile is smoothed according to

$$V_g(y) = \mathcal{F}^{-1} \left[e^{-|q|z_0} \mathcal{F} \left[\sum_{j=1}^{N_g} V_j \chi_j(y) \right] \right], \quad (2)$$

where \mathcal{F} and \mathcal{F}^{-1} are Fourier transform and inverse Fourier transform in the variables y and q , respectively, and $\chi_j(y)$ is the characteristic function of gate j , i.e., $\chi_j(y)$ is 1 if y lies in the region of gate j and 0 otherwise.

We first consider a strictly one-dimension model for the hybrid wire, and generalize to a more realistic two-dimensional model later. The Majorana wire consisting of a semiconductor with Rashba spin-orbit coupling α_R and a proximity induced s-wave gap Δ is described in the Nambu basis $(d_{\uparrow}^{\dagger}(y), d_{\downarrow}^{\dagger}(y), d_{\downarrow}(y), -d_{\uparrow}(y))$ by the Hamiltonian

$$\mathcal{H}_{\text{wire}} = \tau_z \left[-\frac{\hbar^2 \partial_y^2}{2m^*} \sigma_0 - \mu \sigma_0 - i\hbar \alpha_R \sigma_x \partial_y + \delta_{\text{dis}}(y) \sigma_0 + V_g(y) \sigma_0 + V_{\text{conf}}(y) \sigma_0 \right] - E_z \tau_0 \sigma_z + \Delta \tau_x \sigma_0, \quad (3)$$

with disorder potential δ_{dis} , confinement potential V_{conf} , gate potential V_g (see Eq. (2)), and Pauli matrices σ_i and τ_i acting in spin and particle-hole space, respectively. Rashba spin-orbit coupling defines a characteristic energy scale $E_{\text{so}} = \alpha_R^2 m^* / 2 = 0.05 \text{ meV}$ and length scale $l_{\text{so}} = \hbar / (\alpha_R m^*) = 0.19 \mu\text{m}$ of the system, where $\hbar \alpha_R = 0.2 \text{ eV \AA}$ and $m^* = 0.02 m_e$ are realistic values for InAs [29, 35]. Throughout this paper, we consider wires of length $L = 13 l_{\text{so}}$ on a grid with spacing $a = 0.026 l_{\text{so}}$. We use a chemical potential $\mu = 1 E_{\text{so}}$, a Zeeman energy $E_z = 6 E_{\text{so}}$, and gap $\Delta = 2 E_{\text{so}}$, such that the system in the absence of disorder and gate voltages is in the topological regime.

We describe disorder in the wire by first drawing random numbers δ with standard deviation σ_{dis} from a normal distribution and then introduce a finite correlation length λ_{dis} by damping high Fourier modes according to

$$\delta_{\text{dis}}(y) = \mathcal{F}^{-1} \left[e^{-|q|\lambda_{\text{dis}}} \mathcal{F}[\delta(y)] \right]. \quad (4)$$

Here the case $\lambda_{\text{dis}} = 0$ corresponds to onsite disorder.

Wire and leads are connected via steep tunnel barriers of shape $V_{\sigma, V_0}(y) = V_0 \exp[-y^2/(2\sigma^2)]$ with $\sigma = 0.1 l_{\text{so}}$ and $V_0 = 65 E_{\text{so}}$ which we assume to be defined by separate gates that are not included in the optimization. For simplicity, we assume that the leads are normal conducting and without spin orbit coupling. We treat Coulomb blockade in the Majorana wire using a mean-field approximation, such that adding an electron to the system of N_0 electrons costs an additional charging energy $E_c = 8 E_{\text{so}}$, and introduce effective energy levels $\varepsilon_{\text{eff}, i}$ containing both charging energy and single particle energies. We consider the system to be tuned to the center between the conductance resonances for a fixed particle number N_0 in the Majorana wire.

Finally, using the Weidenmüller formula [83]

$$\mathbf{T} = i\varphi_R^{\dagger} \Gamma_R U_w \frac{1}{\varepsilon - \text{diag}(\varepsilon_{\text{eff}}) - U_w^{\dagger} \Sigma U_w} U_w^{\dagger} \Gamma_L \varphi_L, \quad (5)$$

with eigenvectors U_w of the wire Hamiltonian Eq. (3), we can determine the transmission amplitude $A = |T_{\uparrow\uparrow} + T_{\downarrow\downarrow}|$

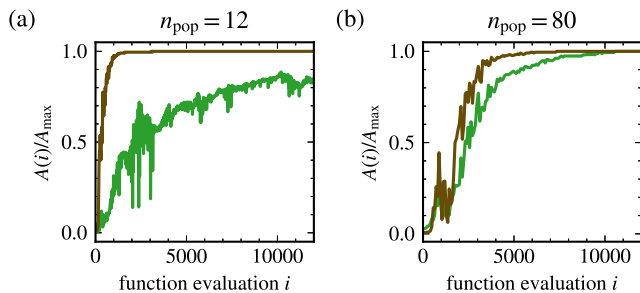


Figure 3. Convergence speed of the CMA-ES algorithm in the presence of disorder using 20 gates. We consider runs of the CMA-ES algorithm with population sizes (a) $n_{\text{pop}} = 12$ and (b) $n_{\text{pop}} = 80$. In both cases, we consider a “hard” problem (green) with onsite disorder, and an “easier” problem with short range disorder correlations $\lambda_{\text{dis}} = 0.052 l_{\text{so}}$. The panels depict the degree of convergence $A(i)/A_{\text{max}}$ as a function of the number of function evaluations i (number of amplitude measurements) where A_{max} is the value to which the amplitude ultimately converges.

in the middle between conductance resonances. Here, ε is the energy of incoming electrons in the lead, and self-energies Σ_{α} , $\Gamma_{\alpha} = i(\Sigma_{\alpha} - \Sigma_{\alpha}^{\dagger})$, $\Sigma = \sum_{\alpha} \Sigma_{\alpha}$, and propagating modes φ_{α} of lead α are obtained by using the Python package KWANT [84].

A finite temperature can be considered by computing the scattering matrix for different thermal excitations of the wire and thermally averaging the transmission amplitude. Then, the transmission amplitude vanishes in the case of trivial ABSs [80, 82], such that our metric is able to distinguish true MZM from an ABS. For the optimization, we consider transport through the first 10 levels and verify the final results by taking into account 50 levels. We carefully checked that this does not influence the optimization results.

In the absence of disorder and with zero voltage at all gates, the lowest level of the wire is approximately at zero energy in the middle of the topological gap (see Fig. 2c), and the associated wave function $\Psi_0 = (\mathbf{u}_0, \mathbf{v}_0)$ is localized at the wire ends and satisfies the Majorana condition $|\mathbf{u}_0(y)| = |\mathbf{v}_0(y)|$ (Fig. 2a). However, if one adds strong disorder (Fig. 2d), both topological gap (red circles, Fig. 2c) and MZMs (Fig. 2b) are destroyed. As a result, the associated transmission amplitude is reduced by two orders of magnitude as compared to the clean wire.

Optimization results: To understand the convergence behavior and the influence of the population size n_{pop} on the CMA-ES algorithm, we consider two scenarios: (i) disorder with a finite correlation length $\lambda_{\text{dis}} = 0.052 l_{\text{so}}$ and (ii) onsite disorder. For both cases, we perform a CMA-ES optimization of 20 gates with population sizes $n_{\text{pop}} = 12$ and $n_{\text{pop}} = 80$. In the easier case (i) already the smaller population size is sufficient to achieve fast convergence after less than 1000 function evalua-

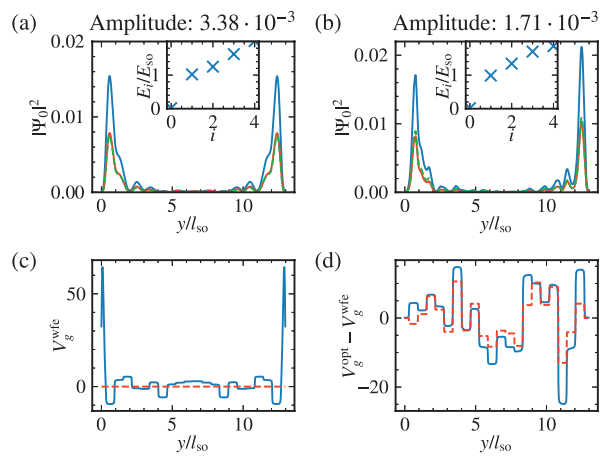


Figure 4. Optimization of transmission via tuning of 20 gates for a one-dimensional wire in the topological regime with $n_{\text{pop}} = 80$. Wave function $|\Psi_0|^2$ of the Majorana level (blue), and the corresponding hole and electron wave functions $|\mathbf{v}_0|^2$ (orange), $|\mathbf{u}_0|^2$ (green) for (a) no disorder in the wire and (b) disorder strength $\sigma_{\text{dis}} = 50 E_{\text{so}}$ and a correlation length $\lambda_{\text{dis}} = 0.052 l_{\text{so}}$. The insets depict the energies of the lowest five Bogoliubov levels. Optimized gate potentials in the absence of disorder are shown in (c), and in (d) the difference between optimized potential obtained with and without disorder is shown. The dashed, red line shows the negative average $-V_{\text{dis}}^{\text{avg}}$ of the disorder potential over the gates, indicating that the algorithm has learned the shape of the disorder potential.

tions (brown line Fig. 3a), whereas for $n_{\text{pop}} = 80$ about five times as many evaluations are necessary (brown line Fig. 3b). In contrast, we find that the more difficult problem (ii) converges poorly in the case of small population sizes, but converges almost as fast as the correlated disorder case for $n_{\text{pop}} = 80$. Thus, if the primary time effort is to perform a function evaluation, i.e., a measurement of the metric in the experiment, we recommend to deviate from the standard value $n_{\text{pop}} = 4 + 3 \ln(N_g - 1)$ [85] for the case of a small disorder correlation length.

We distinguish between two different types of optimizations in the following: (i) optimization in the absence of disorder to determine what shape a potential should have to improve the localization properties of the MZMs (“wave function engineering”), and (ii) optimization with disorder in the wire. In the case of wave function engineering for 20 gates, we find an enhancement of the transmission amplitude by a factor of about 1.6 by optimizing the localization of the MZMs (Fig. 4a) while keeping a sizable topological gap (inset). To achieve this, potentials of the outermost gates are lowered to draw more weight of the wave functions to the wire ends (Fig. 4c, [86]). In case (ii) with disorder (c.f. Fig. 2b), the optimization almost completely restores the MZMs and the topological gap, increasing the transmission amplitude by two orders of magnitude (Fig. 4b). This is achieved by the optimized potential compensating the

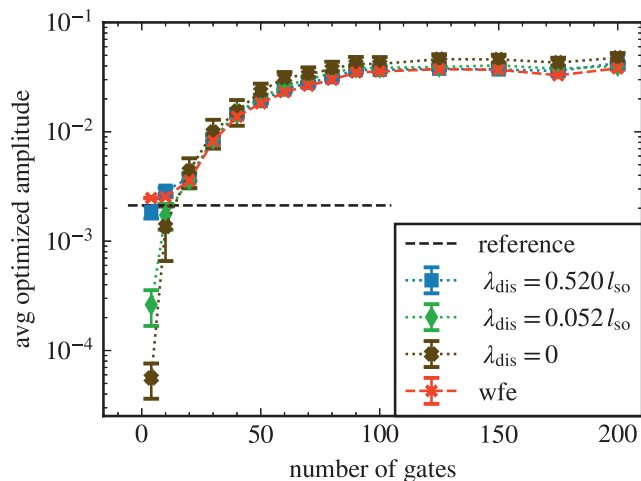


Figure 5. Optimized transmission amplitude as a function of the number of gates along the wire. Results are shown for disorder strength $\sigma_{\text{dis}} = 50 E_{\text{so}}$ and correlation lengths $\lambda_{\text{dis}} = 0.52 l_{\text{so}}$ (blue squares), $0.052 l_{\text{so}}$ (green diamonds), 0 (onsite disorder, brown crosses). Red crosses indicate the wave function engineering result obtained for optimization without any disorder in the wire. We show averages over ten realizations of disorder in each case, and an average over 10 seeds of the CMA-ES algorithm in the absence of disorder. The black dashed line shows the reference value obtained without disorder and no optimization.

average disorder (dashed red line Fig. 4d), in addition to the zero disorder optimal values (Fig. 4d). We emphasize that the CMA-ES algorithm has no knowledge about system parameters, but only suggests gate configurations based on corresponding transmission amplitudes.

Having seen from the examples how optimization can make MZMs more robust, we next consider how reliable the optimization is for different disorder correlation lengths, how many gates are necessary, and how strong the dependence on the seed of the CMA-ES random number generator is. For this, we consider 15 different values for the number of gates, from $N_g = 4$ to $N_g = 200$, and three types of disorder, onsite ($\lambda_{\text{dis}} = 0$), $\lambda_{\text{dis}} = 0.052 l_{\text{so}}$ and $\lambda_{\text{dis}} = 0.52 l_{\text{so}}$, as well as wave function engineering without disorder. For the case with disorder, we consider ten different disorder realizations and average the resulting amplitudes, while in the absence of disorder we average over ten different seeds of the CMA-ES algorithm. We find that for at least 20 gates all considered disorder profiles can be compensated reliably (see Fig. 5). For too few gates $N_g \leq 10$, it is no longer possible to remove disorder with very small correlation length. For many gates, $N_g \approx 100$, the amplitude saturates, having increased by one order of magnitude as compared to $N_g = 20$, but with the drawback that up to 10^5 function evaluations are needed to achieve full convergence. We observe a sweet spot $20 \leq N_g \leq 50$, where the number of necessary function evaluations is acceptable and still significant im-

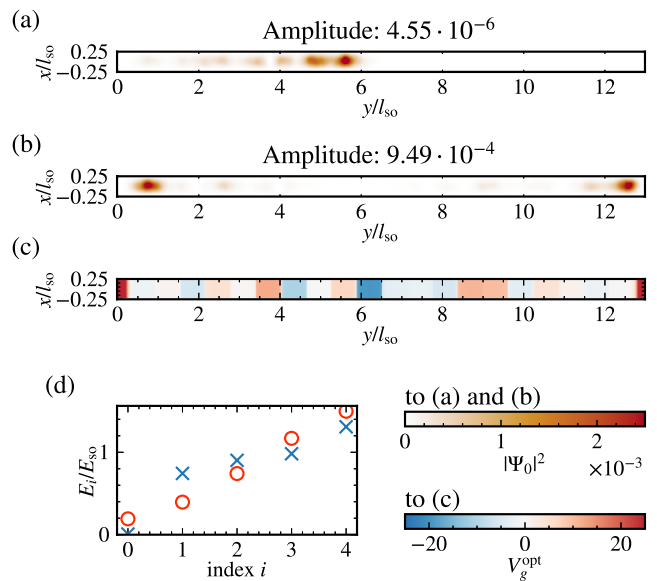


Figure 6. Optimization of 20 gates along a two-dimensional wire in the topological regime. Wave function $|\Psi_0|^2$ of the lowest level for (a) disorder with $\sigma_{\text{dis}} = 150 E_{\text{so}}$ and $\lambda_{\text{dis}} = 0.052 l_{\text{so}}$ where all gates are set to zero for reference and (b) optimized gates in presence of disorder. (c) CMA-ES optimization result for the gate potential that maximizes the transmission amplitude. (d) Energies of the lowest ten Bogoliubov levels for the reference case with disorder (red circles) and for the optimized gate potential (blue crosses). Similarly to the one dimensional case, the Majorana zero modes, topological gap, and transmission amplitude are restored by the optimized gates.

provements of the amplitude and complete compensation of disorder are possible.

Choice of metric: Above, we have chosen the coherent transmission amplitude, since it distinguishes ABS from MZMs [80, 82] and benefits from enhanced localization of MZMs. For a Majorana wire, other metrics come to mind that may be easier to determine experimentally, which however turn out to cause problems in the optimization process. For example, optimizing the gap $|\varepsilon_1 - \varepsilon_0|$ has the disadvantage that it does not require ε_0 to be small and in addition does not depend on the localization at the wire ends. On the other hand, when minimizing the lowest level ε_0 , localization of MZMs is not strengthened, and in addition one is not able to exclude a vanishing gap or the presence of ABSs. Optimizing the incoherent part of the conductance through the wire produces trivial ABSs instead of MZMs by lowering the outermost gates [86] to create potential wells at the ends [68], while increasing the effective chemical potential in the remaining wire, thus lifting it into the trivial regime.

Two dimensional case: We study a wire with length $L_y = 13 l_{\text{so}}$ and width $L_x = 0.39 l_{\text{so}}$, and account for the orbital effect of the magnetic field by adding Peierls phases $e^{-ie/\hbar \int_{\mathbf{r}_1}^{\mathbf{r}_2} \mathbf{A} \cdot d\mathbf{r}}$ to the hoppings from site \mathbf{r}_1 to site

r_2 . We choose a chemical potential $\mu = 63 E_{\text{so}}$ and Zeeman energy $E_z = 6 E_{\text{so}}$ such that the wire in the absence of disorder and gates is in the topological regime with one occupied subband (a discussion of transport through higher subbands can be found in [86]). In the presence of strong disorder, the MZMs are destroyed (Fig. 6a) and the gap collapses (red circles in Fig. 6d), but again optimization with only 20 gates along the wire can restore the MZMs (Fig. 6b) as well as the gap (blue crosses in Fig. 6d) similar to the one dimensional case.

Conclusions: We studied machine learning optimization of a gate array using the CMA-ES algorithm. Using the coherent transmission amplitude through a Coulomb blockaded Majorana wire as metric, we find: (i) optimization in absence of disorder improves localization of MZMs significantly and (ii) optimization even restores MZMs fully in the case of strong disorder that otherwise destroys the topological phase. We discussed the importance of the choice of an appropriate metric, showed that the number of necessary function evaluations would be experimentally feasible, and that a moderate number of gates is sufficient for restoration of MZMs in the presence of disorder.

Acknowledgments: We would like to thank E. van Nieuwenburg and A. Chatterjee for helpful discussions. This work has been funded by the Deutsche Forschungsgemeinschaft (DFG) under Grants No. RO 2247/11-1 and No. 406116891 within the Research Training Group RTG 2522/1.

-
- [1] T. Karzig, C. Knapp, R. M. Lutchyn, P. Bonderson, M. B. Hastings, C. Nayak, J. Alicea, K. Flensberg, S. Plugge, Y. Oreg, C. M. Marcus, and M. H. Freedman, Scalable designs for quasiparticle-poisoning-protected topological quantum computation with Majorana zero modes, *Physical Review B* **95**, 235305 (2017).
- [2] F. Arute, K. Arya, R. Babbush, D. Bacon, J. C. Bardin, R. Barends, R. Biswas, S. Boixo, Brandao, Fernando G. S. L., D. A. Buell, B. Burkett, Y. Chen, Z. Chen, B. Chiaro, R. Collins, W. Courtney, A. Dunsworth, E. Farhi, B. Foxen, A. Fowler, C. Gidney, M. Giustina, R. Graff, K. Guerin, S. Habegger, M. P. Harrigan, M. J. Hartmann, A. Ho, M. Hoffmann, T. Huang, T. S. Humble, S. V. Isakov, E. Jeffrey, Z. Jiang, D. Kafri, K. Kechedzhi, J. Kelly, P. V. Klimov, S. Knysh, A. Korotkov, F. Kostritsa, D. Landhuis, M. Lindmark, E. Lucero, D. Lyakh, S. Mandrà, J. R. McClean, M. McEwen, A. Megrant, X. Mi, K. Michielsen, M. Mohseni, J. Mutus, O. Naaman, M. Neeley, C. Neill, M. Y. Niu, E. Ostby, A. Petukhov, J. C. Platt, C. Quintana, E. G. Rieffel, P. Roushan, N. C. Rubin, D. Sank, K. J. Satzinger, V. Smelyanskiy, K. J. Sung, M. D. Trevithick, A. Vainsencher, B. Villalonga, T. White, Z. J. Yao, P. Yeh, A. Zalcman, H. Neven, and J. M. Martinis, Quantum supremacy using a programmable superconducting processor, *Nature* **574**, 505 (2019).
- [3] D. T. Lennon, H. Moon, L. C. Camenzind, L. Yu, D. M. Zumbühl, G. A. D. Briggs, M. A. Osborne, E. A. Laird, and N. Ares, Efficiently measuring a quantum device using machine learning, *npj Quantum Information* **5**, 1 (2019).
- [4] Y. Oreg and F. von Oppen, Majorana Zero Modes in Networks of Cooper-Pair Boxes: Topologically Ordered States and Topological Quantum Computation, *Annual Review of Condensed Matter Physics* **11**, 397 (2020).
- [5] N. Ares, Machine learning as an enabler of qubit scalability, *Nature Reviews Materials* **6**, 870 (2021).
- [6] T. A. Baart, P. T. Eendebak, C. Reichl, W. Wegscheider, and L. M. K. Vandersypen, Computer-automated tuning of semiconductor double quantum dots into the single-electron regime, *Applied Physics Letters* **108**, 213104 (2016).
- [7] D. L. Craig, H. Moon, F. Fedele, D. T. Lennon, B. van Straaten, F. Vigneau, L. C. Camenzind, D. M. Zumbühl, G. A. D. Briggs, M. A. Osborne, D. Sejdinovic, and N. Ares, Bridging the reality gap in quantum devices with physics-aware machine learning.
- [8] J. Ziegler, T. McJunkin, E. S. Joseph, S. S. Kalantre, B. Harpt, D. E. Savage, M. G. Lagally, M. A. Eriksson, J. M. Taylor, and J. P. Zvolak, Toward Robust Autotuning of Noisy Quantum Dot Devices.
- [9] A. Frees, J. K. Gamble, D. R. Ward, R. Blume-Kohout, M. A. Eriksson, M. Friesen, and S. N. Coppersmith, Compressed Optimization of Device Architectures for Semiconductor Quantum Devices, *Physical Review Applied* **11**, 024063 (2019).
- [10] S. S. Kalantre, J. P. Zvolak, S. Ragole, X. Wu, N. M. Zimmerman, M. D. Stewart, and J. M. Taylor, Machine learning techniques for state recognition and auto-tuning in quantum dots, *npj Quantum Information* **5**, 1 (2019).
- [11] H. Moon, D. T. Lennon, J. Kirkpatrick, N. M. van Esbroeck, L. C. Camenzind, L. Yu, F. Vigneau, D. M. Zumbühl, G. A. D. Briggs, M. A. Osborne, D. Sejdinovic, E. A. Laird, and N. Ares, Machine learning enables completely automatic tuning of a quantum device faster than human experts, *Nature Communications* **11**, 4161 (2020).
- [12] H.-C. Ruiz Euler, M. N. Boon, J. T. Wildeboer, B. van de Ven, T. Chen, H. Broersma, P. A. Bobbert, and W. G. van der Wiel, A deep-learning approach to realizing functionality in nanoelectronic devices, *Nature Nanotechnology* **15**, 992 (2020).
- [13] T. D. Ladd, F. Jelezko, R. Laflamme, Y. Nakamura, C. Monroe, and J. L. O'Brien, Quantum computers, *Nature* **464**, 45 (2010).
- [14] R. Hanson, L. P. Kouwenhoven, J. R. Petta, S. Tarucha, and L. M. K. Vandersypen, Spins in few-electron quantum dots, *Reviews of Modern Physics* **79**, 1217 (2007).
- [15] C. Kloeffel and D. Loss, Prospects for Spin-Based Quantum Computing in Quantum Dots, *Annual Review of Condensed Matter Physics* **4**, 51 (2013).
- [16] L. M. K. Vandersypen, H. Bluhm, J. S. Clarke, A. S. Dzurak, R. Ishihara, A. Morello, D. J. Reilly, L. R. Schreiber, and M. Veldhorst, Interfacing spin qubits in quantum dots and donors—hot, dense, and coherent, *npj Quantum Information* **3**, 1 (2017).
- [17] T. Botzem, M. D. Shulman, S. Foletti, S. P. Harvey, O. E. Dial, P. Bethke, P. Cerfontaine, R. P. G. McNeil, D. Mahalu, V. Umansky, A. Ludwig, A. Wieck, D. Schuh, D. Bougeard, A. Yacoby, and H. Bluhm, Tuning Methods

- for Semiconductor Spin Qubits, *Physical Review Applied* **10**, 10.1103/PhysRevApplied.10.054026 (2018).
- [18] J. D. Teske, S. S. Humpohl, R. Otten, P. Bethke, P. Cerverfontaine, J. Dedden, A. Ludwig, A. D. Wieck, and H. Bluhm, A machine learning approach for automated fine-tuning of semiconductor spin qubits, *Applied Physics Letters* **114**, 133102 (2019).
- [19] A. R. Mills, M. M. Feldman, C. Monical, P. J. Lewis, K. W. Larson, A. M. Mounce, and J. R. Petta, Computer-automated tuning procedures for semiconductor quantum dot arrays, *Applied Physics Letters* **115**, 113501 (2019).
- [20] R. Durrer, B. Kratochwil, J. V. Koski, A. J. Landig, C. Reichl, W. Wegscheider, T. Ihn, and E. Greplová, Automated Tuning of Double Quantum Dots into Specific Charge States Using Neural Networks, *Physical Review Applied* **13**, 054019 (2020).
- [21] N. M. van Esbroeck, D. T. Lennon, H. Moon, V. Nguyen, F. Vigneau, L. C. Camenzind, L. Yu, D. M. Zumbühl, G. A. D. Briggs, D. Sejdinovic, and N. Ares, Quantum device fine-tuning using unsupervised embedding learning, *New Journal of Physics* **22**, 095003 (2020).
- [22] F. Fedele, A. Chatterjee, S. Fallahi, G. C. Gardner, M. J. Manfra, and F. Kuemmeth, Simultaneous Operations in a Two-Dimensional Array of Singlet-Triplet Qubits, *PRX Quantum* **2**, 040306 (2021).
- [23] O. Krause, A. Chatterjee, F. Kuemmeth, and E. van Nieuwenburg, Learning coulomb diamonds in large quantum dot arrays, arXiv preprint arXiv:2205.01443 (2022).
- [24] J. Alicea, Y. Oreg, G. Refael, F. von Oppen, and M. P. A. Fisher, Non-Abelian statistics and topological quantum information processing in 1D wire networks, *Nature Physics* **7**, 412 (2011).
- [25] D. J. Clarke, J. D. Sau, and S. Tewari, Majorana fermion exchange in quasi-one-dimensional networks, *Physical Review B* **84**, 035120 (2011).
- [26] T. Hyart, B. van Heck, I. C. Fulga, M. Burrello, A. R. Akhmerov, and C. W. J. Beenakker, Flux-controlled quantum computation with Majorana fermions, *Physical Review B* **88**, 035121 (2013).
- [27] S. D. Sarma, M. Freedman, and C. Nayak, Majorana zero modes and topological quantum computation, *npj Quantum Information* **1**, 1 (2015).
- [28] D. Aasen, M. Hell, R. V. Mishmash, A. Higginbotham, J. Danon, M. Leijnse, T. S. Jespersen, J. A. Folk, C. M. Marcus, K. Flensberg, and J. Alicea, Milestones Toward Majorana-Based Quantum Computing, *Physical Review X* **6**, 031016 (2016).
- [29] R. M. Lutchyn, Bakkers, E. P. A. M., L. P. Kouwenhoven, P. Krogstrup, C. M. Marcus, and Y. Oreg, Majorana zero modes in superconductor–semiconductor heterostructures, *Nature Reviews Materials* **3**, 52 (2018).
- [30] S. Vijay and L. Fu, Teleportation-based quantum information processing with Majorana zero modes, *Physical Review B* **94**, 235446 (2016).
- [31] A. Y. Kitaev, Unpaired Majorana fermions in quantum wires, *Physics-Uspekhi* **44**, 131 (2001).
- [32] R. M. Lutchyn, J. D. Sau, and S. Das Sarma, Majorana fermions and a topological phase transition in semiconductor-superconductor heterostructures, *Physical review letters* **105**, 077001 (2010).
- [33] Y. Oreg, G. Refael, and F. von Oppen, Helical liquids and Majorana bound states in quantum wires, *Physical review letters* **105**, 177002 (2010).
- [34] J. D. Sau, S. Tewari, R. M. Lutchyn, T. D. Stanescu, and S. Das Sarma, Non-Abelian quantum order in spin-orbit-coupled semiconductors: Search for topological Majorana particles in solid-state systems, *Physical Review B* **82**, 214509 (2010).
- [35] V. Mourik, K. Zuo, S. M. Frolov, S. R. Plissard, Bakkers, E. P. A. M., and L. P. Kouwenhoven, Signatures of Majorana fermions in hybrid superconductor-semiconductor nanowire devices, *Science (New York, N.Y.)* **336**, 1003 (2012).
- [36] A. Das, Y. Ronen, Y. Most, Y. Oreg, M. Heiblum, and H. Shtrikman, Zero-bias peaks and splitting in an Al–InAs nanowire topological superconductor as a signature of Majorana fermions, *Nature Physics* **8**, 887 (2012).
- [37] M. T. Deng, C. L. Yu, G. Y. Huang, M. Larsson, P. Caroff, and H. Q. Xu, Anomalous zero-bias conductance peak in a Nb–InSb nanowire–Nb hybrid device, *Nano Letters* **12**, 6414 (2012).
- [38] F. Nichele, A. C. C. Drachmann, A. M. Whiticar, E. C. T. O’Farrell, H. J. Suominen, A. Fornieri, T. Wang, G. C. Gardner, C. Thomas, A. T. Hatke, P. Krogstrup, M. J. Manfra, K. Flensberg, and C. M. Marcus, Scaling of Majorana Zero-Bias Conductance Peaks, *Physical review letters* **119**, 136803 (2017).
- [39] L. P. Rokhinson, X. Liu, and J. K. Furdyna, The fractional a.c. Josephson effect in a semiconductor–superconductor nanowire as a signature of Majorana particles, *Nature Physics* **8**, 795 (2012).
- [40] S. M. Albrecht, A. P. Higginbotham, M. Madsen, F. Kuemmeth, T. S. Jespersen, J. Nygård, P. Krogstrup, and C. M. Marcus, Exponential protection of zero modes in Majorana islands, *Nature* **531**, 206 (2016).
- [41] S. Boutin, J. Camirand Lemyre, and I. Garate, Majorana bound state engineering via efficient real-space parameter optimization, *Physical Review B* **98**, 214512 (2018).
- [42] J. Klinovaja, P. Stano, and D. Loss, Transition from fractional to majorana fermions in rashba nanowires, *Physical review letters* **109**, 236801 (2012).
- [43] N. Mohanta, T. Zhou, J.-W. Xu, J. E. Han, A. D. Kent, J. Shabani, I. Žutić, and A. Matos-Abiad, Electrical Control of Majorana Bound States Using Magnetic Stripes, *Physical Review Applied* **12**, 034048 (2019).
- [44] S. Turcotte, S. Boutin, J. C. Lemyre, I. Garate, and M. Pioro-Ladrière, Optimized micromagnet geometries for Majorana zero modes in low g-factor materials, *Physical Review B* **102**, 125425 (2020).
- [45] A. Melo, T. Tanev, and A. R. Akhmerov, Greedy optimization of the geometry of majorana josephson junctions, arXiv preprint arXiv:2205.05689 (2022).
- [46] H. Zhang, Ö. Gül, S. Conesa-Boj, M. P. Nowak, M. Wimmer, K. Zuo, V. Mourik, F. K. de Vries, J. van Veen, M. W. A. de Moor, J. D. S. Bommer, D. J. van Woerkom, D. Car, S. R. Plissard, E. P. A. M. Bakkers, M. Quintero-Pérez, M. C. Cassidy, S. Koelling, S. Goswami, K. Watanabe, T. Taniguchi, and L. P. Kouwenhoven, Ballistic superconductivity in semiconductor nanowires, *Nature Communications* **8**, 16025 (2017).
- [47] S. Ahn, H. Pan, B. Woods, T. D. Stanescu, and S. D. Sarma, Estimating disorder and its adverse effects in semiconductor Majorana nanowires, arXiv:2109.00007 (2021).
- [48] S. Das Sarma and H. Pan, Disorder-induced zero-bias

- peaks in Majorana nanowires, *Physical Review B* **103**, 195158 (2021).
- [49] P. Yu, J. Chen, M. Gomanko, G. Badawy, Bakkers, E. P. A. M., K. Zuo, V. Mourik, and S. M. Frolov, Non-Majorana states yield nearly quantized conductance in proximatized nanowires, *Nature Physics* **17**, 482 (2021).
- [50] D. Bagrets and A. Altland, Class D spectral peak in Majorana quantum wires, *Physical review letters* **109**, 227005 (2012).
- [51] D. I. Pikulin, J. P. Dahlhaus, M. Wimmer, H. Schomerus, and C. W. J. Beenakker, A zero-voltage conductance peak from weak antilocalization in a Majorana nanowire, *New Journal of Physics* **14**, 125011 (2012).
- [52] J. Liu, A. C. Potter, K. T. Law, and P. A. Lee, Zero-bias peaks in the tunneling conductance of spin-orbit-coupled superconducting wires with and without Majorana end-states, *Physical review letters* **109**, 267002 (2012).
- [53] H. Pan and S. Das Sarma, Physical mechanisms for zero-bias conductance peaks in Majorana nanowires, *Physical Review Research* **2**, 013377 (2020).
- [54] S. Takei, B. M. Fregoso, H.-Y. Hui, A. M. Lobos, and S. Das Sarma, Soft superconducting gap in semiconductor Majorana nanowires, *Physical review letters* **110**, 186803 (2013).
- [55] N. Hansen and A. Ostermeier, Completely derandomized self-adaptation in evolution strategies, *Evolutionary Computation* **9**, 159 (2001).
- [56] N. Hansen, S. D. Müller, and P. Koumoutsakos, Reducing the time complexity of the derandomized evolution strategy with covariance matrix adaptation (CMA-ES), *Evolutionary Computation* **11**, 1 (2003).
- [57] N. Hansen, *The CMA Evolution Strategy: A Comparing Review*, in *Towards a New Evolutionary Computation*, Studies in Fuzziness and Soft Computing, edited by J. A. Lozano, E. Bengoetxea, I. Inza, and P. Larrañaga (Springer-Verlag Berlin Heidelberg, Berlin, Heidelberg, 2006) pp. 75–102.
- [58] J. A. Lozano, E. Bengoetxea, I. Inza, and P. Larrañaga, eds., *Towards a New Evolutionary Computation: Advances in the Estimation of Distribution Algorithms*, Studies in Fuzziness and Soft Computing, Vol. 192 (Springer-Verlag Berlin Heidelberg, Berlin, Heidelberg, 2006).
- [59] I. Loshchilov and F. Hutter, CMA-ES for Hyperparameter Optimization of Deep Neural Networks, arxiv:1604.07269 (2016).
- [60] M. Willjuice Iruthayarajan and S. Baskar, Covariance matrix adaptation evolution strategy based design of centralized PID controller, *Expert Systems with Applications* **37**, 5775 (2010).
- [61] I. Loshchilov, M. Schoenauer, and M. Sebag, Bipopulation cma-es algorithms with surrogate models and line searches, in *Proceedings of the 15th annual conference companion on Genetic and evolutionary computation* (2013) pp. 1177–1184.
- [62] G. Kells, D. Meidan, and P. Brouwer, Near-zero-energy end states in topologically trivial spin-orbit coupled superconducting nanowires with a smooth confinement, *Physical Review B* **86**, 100503 (2012).
- [63] E. Prada, P. San-Jose, and R. Aguado, Transport spectroscopy of n s nanowire junctions with majorana fermions, *Physical Review B* **86**, 180503 (2012).
- [64] D. Rainis, L. Trifunovic, J. Klinovaja, and D. Loss, Towards a realistic transport modeling in a superconducting nanowire with Majorana fermions, *Physical Review B* **87**, 024515 (2013).
- [65] J. Cayao, E. Prada, P. San-Jose, and R. Aguado, Sns junctions in nanowires with spin-orbit coupling: Role of confinement and helicity on the subgap spectrum, *Physical Review B* **91**, 024514 (2015).
- [66] P. San-Jose, J. Cayao, E. Prada, and R. Aguado, Majorana bound states from exceptional points in non-topological superconductors, *Scientific reports* **6**, 1 (2016).
- [67] J. Chen, P. Yu, J. Stenger, M. Hocevar, D. Car, S. R. Plissard, E. P. A. M. Bakkers, T. D. Stanescu, and S. M. Frolov, Experimental phase diagram of zero-bias conductance peaks in superconductor/semiconductor nanowire devices, *Science advances* **3**, e1701476 (2017).
- [68] C.-X. Liu, J. D. Sau, T. D. Stanescu, and S. Das Sarma, Andreev bound states versus Majorana bound states in quantum dot-nanowire-superconductor hybrid structures: Trivial versus topological zero-bias conductance peaks, *Physical Review B* **96**, 075161 (2017).
- [69] F. Peñaranda, R. Aguado, P. San-Jose, and E. Prada, Quantifying wave-function overlaps in inhomogeneous majorana nanowires, *Physical Review B* **98**, 235406 (2018).
- [70] J. Avila, F. Peñaranda, E. Prada, P. San-Jose, and R. Aguado, Non-hermitian topology as a unifying framework for the andreev versus majorana states controversy, *Communications Physics* **2**, 1 (2019).
- [71] C.-K. Chiu and S. Das Sarma, Fractional Josephson effect with and without Majorana zero modes, *Physical Review B* **99**, 035312 (2019).
- [72] J. Chen, B. D. Woods, P. Yu, M. Hocevar, D. Car, S. R. Plissard, Bakkers, E. P. A. M., T. D. Stanescu, and S. M. Frolov, Ubiquitous Non-Majorana Zero-Bias Conductance Peaks in Nanowire Devices, *Physical review letters* **123**, 107703 (2019).
- [73] B. D. Woods, J. Chen, S. M. Frolov, and T. D. Stanescu, Zero-energy pinning of topologically trivial bound states in multiband semiconductor-superconductor nanowires, *Physical Review B* **100**, 125407 (2019).
- [74] A. Vuik, B. Nijholt, A. Akhmerov, and M. Wimmer, Reproducing topological properties with quasi-Majorana states, *SciPost Physics* **7**, 061 (2019).
- [75] O. Dmytruk, D. Loss, and J. Klinovaja, Pinning of andreev bound states to zero energy in two-dimensional superconductor-semiconductor rashba heterostructures, *Physical Review B* **102**, 245431 (2020).
- [76] E. Prada, P. San-Jose, M. W. de Moor, A. Geresdi, E. J. Lee, J. Klinovaja, D. Loss, J. Nygård, R. Aguado, and L. P. Kouwenhoven, From andreev to majorana bound states in hybrid superconductor-semiconductor nanowires, *Nature Reviews Physics* **2**, 575 (2020).
- [77] M. Valentini, F. Peñaranda, A. Hofmann, M. Brauns, R. Hauschild, P. Krogstrup, P. San-Jose, E. Prada, R. Aguado, and G. Katsaros, Nontopological zero-bias peaks in full-shell nanowires induced by flux-tunable andreev states, *Science* **373**, 82 (2021).
- [78] H. Zhang, M. W. A. de Moor, J. D. S. Bommer, Di Xu, G. Wang, N. van Loo, C.-X. Liu, S. Gazibegovic, J. A. Logan, D. Car, Veld, Roy L. M. Op het, P. J. van Veldhoven, S. Koelling, M. A. Verheijen, M. Pendharkar, D. J. Pennachio, B. Shojaei, J. S. Lee, C. J. Palmstrøm, E. P. A. M. Bakkers, S. D. Sarma, and L. P. Kouwenhoven, Large zero-bias peaks in InSb-Al hybrid semiconductor-

superconductor nanowire devices.

- [79] L. Fu, Electron teleportation via Majorana bound states in a mesoscopic superconductor, *Physical review letters* **104**, 056402 (2010).
- [80] M. Hell, K. Flensberg, and M. Leijnse, Distinguishing Majorana bound states from localized Andreev bound states by interferometry, *Physical Review B* **97**, 161401 (2018).
- [81] A. M. Whiticar, A. Fornieri, E. C. T. O’Farrell, A. C. C. Drachmann, T. Wang, C. Thomas, S. Gronin, R. Kallagher, G. C. Gardner, M. J. Manfra, C. M. Marcus, and F. Nichele, Coherent transport through a Majorana island in an Aharonov-Bohm interferometer, *Nature Communications* **11**, 3212 (2020).
- [82] M. Thamm and B. Rosenow, Transmission amplitude through a Coulomb blockaded Majorana wire, *Physical Review Research* **3**, 023221 (2021).
- [83] C. Mahaux and H. A. Weidenmüller, Comparison between the R-matrix and eigenchannel methods, *Physical Review* **170**, 847 (1968).
- [84] C. W. Groth, M. Wimmer, A. R. Akhmerov, and X. Waintal, Kwant: a software package for quantum transport, *New Journal of Physics* **16**, 063065 (2014).
- [85] N. Hansen, Y. Akimoto, and P. Baudis, CMA-ES/pycma on Github, Zenodo, 10.5281/zenodo.2559634 (2019).
- [86] See supplemental material.

Supplementary Material: Machine learning optimization of Majorana hybrid nanowires

Matthias Thamm and Bernd Rosenow

Institut für Theoretische Physik, Universität Leipzig, Brüderstrasse 16, 04103 Leipzig, Germany

A. AMPLITUDE OF COHERENT TRANSMISSION

As a metric for optimization, we use the amplitude of coherent transmission $|T_{\uparrow\uparrow} + T_{\downarrow\downarrow}|$ through an Aharonov-Bohm interferometer, where $T_{\sigma\sigma}$ is the quantum mechanical amplitude for an electron with spin σ to tunnel through the Majorana wire. The current through the interferometer is in leading order interference given by

$$I = \frac{e^2}{h} \left\{ \sum_{\sigma\sigma'} |T_{\sigma\sigma'}|^2 + 2|T^{\text{ref}}|^2 + I_{\text{intf}} \right\} \quad (\text{S1})$$

$$I_{\text{intf}} = 2 \sum_{\sigma} \text{Re} [e^{i\phi} T_{\sigma\sigma} T^{\text{ref}}] = \frac{e^2}{h} |T^{\text{ref}}| [e^{i\phi} (T_{\uparrow\uparrow} + T_{\downarrow\downarrow}) + e^{-i\phi} (T_{\uparrow\uparrow} + T_{\downarrow\downarrow})^*] \quad (\text{S2})$$

$$= \frac{2e^2}{h} |T^{\text{ref}}| |T_{\uparrow\uparrow} + T_{\downarrow\downarrow}| \cos(\phi + \gamma), \quad (\text{S3})$$

where $T_{\uparrow\uparrow} + T_{\downarrow\downarrow} = |T_{\uparrow\uparrow} + T_{\downarrow\downarrow}| e^{i\gamma}$, the Aharonov-Bohm phase is denoted as ϕ , and the transmission through the reference arm T^{ref} is assumed to be real and diagonal in spin. Hence, the amplitude of interference oscillation is given by $|T_{\uparrow\uparrow} + T_{\downarrow\downarrow}|$.

B. ALTERNATIVE METRICS AND THEIR SHORTCOMINGS

Here, we provide examples of optimizations of alternative metrics whose drawbacks are mentioned in the main text. First, we consider the direct conductance through the wire without an interferometer, which is easier to measure experimentally, but has the disadvantage of not being able to distinguish between ABSs and MZMs. This manifests itself in the optimization by yielding a pair of trivial near-zero energy levels (Fig. S1b), the ABSs, both of which are localized at the wire ends (Fig. S1a).

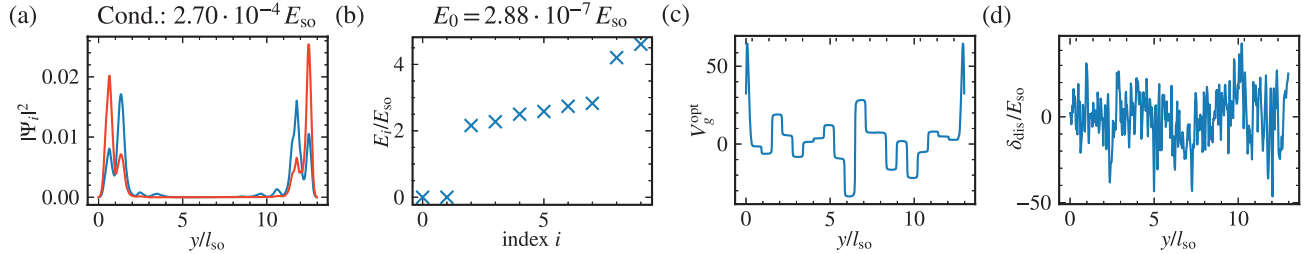


Figure S1. Results for direct conductance optimization in a one dimensional wire in presence of disorder. The direct conductance cannot distinguish between MZMs and ABSs. We use 20 gates of equal size along the wire. (a) Wave function $|\Psi_i|^2$ of the the lowest level $i = 0$ (blue) and the second level $i = 1$ (red). (b) Energies of the lowest ten Bogoliubov levels. (c) CMA-ES optimization result that maximizes the direct conductance. (d) Disorder potential for $\sigma_{\text{dis}} = 50 E_{\text{so}}$ and $\lambda_{\text{dis}} = 0.052 l_{\text{so}}$. With the optimized gates, we observe two near zero energy ABSs and no MZMs.

Another potential metric is the topological gap $|\varepsilon_1 - \varepsilon_0|$, which, however, does not depend on the localization of the MZMs, nor does it rely on the presence of MZMs and the topological phase either. An optimization shows large $|\varepsilon_1 - \varepsilon_0|$ (Fig. S2b), but the associated lowest level is not a Majorana state (Fig. S2a). In addition, $\varepsilon_0 = 1.9 \cdot 10^{-8} E_{\text{so}}$ is also strongly reduced, which also shows that minimizing ε_0 does not favor MZMs and can further be realized with ABSs.

Furthermore, we discussed problems related to suboptimal parameters. For the thermal average to reliably penalize ABSs, the temperature should be sufficiently high, and at the same time, of course, the temperature must be below the

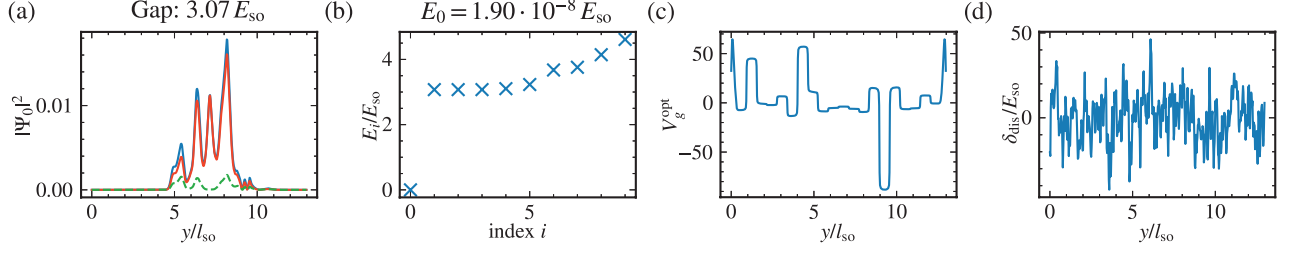


Figure S2. Results for gap optimization in a one dimensional wire in presence of disorder. We define the gap as the difference between the first two energy eigenvalues. We use 20 gates of equal size along the wire. (a) Wave function $|\Psi_0|^2$ of the lowest level and corresponding hole and electron wave functions $|v_0|^2$ (orange) and $|u_0|^2$ (green). (b) Energies of the lowest ten Bogoliubov levels. (c) CMA-ES optimization result that maximizes the gap. (d) Disorder potential for $\sigma_{dis} = 50 E_{so}$ and $\lambda_{dis} = 0.052 l_{so}$. With the optimized gates, we observe an increased gap, however despite the lowest level being close to zero energy it is not a Majorana level as $|u_0| \neq |v_0|$.

critical temperature for preserving superconductivity. If one chooses too small temperatures, for example $T = 34$ mK, the optimization favors ABSs with energy slightly larger than temperature (Fig. S3) and also the gap above the ABS levels can be strongly reduced.

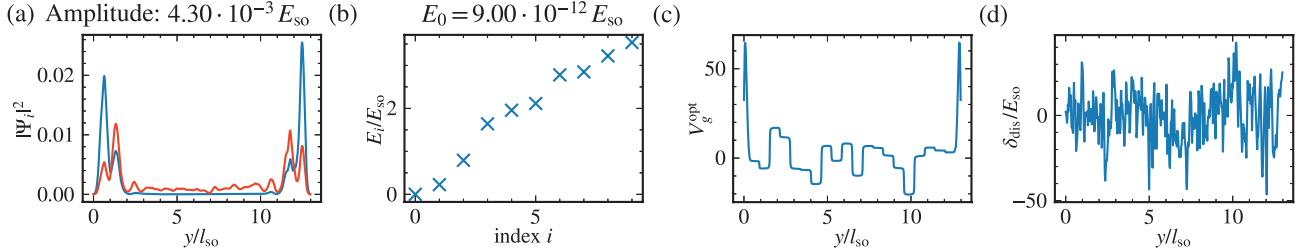


Figure S3. Results for transmission amplitude optimization in a one dimensional wire in presence of disorder but at very low temperature $\beta = 18 E_{so}^{-1}$. At very small temperatures an ABSs with low but finite energy has very different weight than a zero energy ABSs in the thermal average, such that the amplitude does not cancel when there are two ABSs with slightly split energy. We use 20 gates of equal size along the wire. (a) Wave function $|\Psi_i|^2$ of the lowest level $i = 0$ (blue) and the second level $i = 1$ (red). (b) Energies of the lowest ten Bogoliubov levels. (c) CMA-ES optimization result that maximizes the gap. (d) Disorder potential for $\sigma_{dis} = 50 E_{so}$ and $\lambda_{dis} = 0.052 l_{so}$. With the optimized gates, we observe a diminished gap and a pair of ABSs near zero energy which are split by a small energy difference.

C. COMPUTATIONAL DETAILS

We use the pycma [2] python implementation of the CMA-ES [3, 4] algorithm, with an initial configuration $\mathbf{V}_g^{(0)} = 0$, the starting step size $\sigma^{(0)} = 0.1 E_{so}$, population sizes of 80 or $4 + 3 \ln(N_g)$, and a seed of the pseudo random number generator of 12345678, if not specified otherwise. As algorithm termination conditions, we use $topfun = 10^{-15}$, $tolfunhist = 10^{-8}$, and $tolx = 10^{-5} E_{so}$. We note, however, that the potentials do not change significantly anymore much earlier to meeting these conditions, such that one can stop the optimization earlier in an experimental situation.

For the computation of the transmission amplitude, we use KWANT [1] to obtain several quantities. We define the lattice, onsite terms, and hopping terms using KWANT (Fig. S4) and extract the self energies Σ_α of lead α , as well as the propagating modes ϕ_α defined at the lead-wire interfaces. In addition, KWANT allows to extract the wire Hamiltonian \mathcal{H}_{wire} , which we use to compute eigenstates U_w and energy levels ε_w , from which we obtain the effective couplings and energy levels [5] used in the computation of the scattering matrix. For the Majorana wires, we consider an effective mass $m^* = 0.02 m_e$, Rashba spin orbit coupling strength $\hbar\alpha_R = 0.2 \text{ eV\AA}$, a lattice spacing $a = 0.026 l_{so}$, and wire length $L = 13 l_{so}$. In addition, we set the chemical potential $\mu = 1 E_{so}$, the Zeeman energy $E_z = 6 E_{so}$, the proximity s-wave gap $\Delta = 2 E_{so}$, the charging energy $E_c = 8 E_{so}$, and the electron temperature $T = 183 \text{ mK}$. In the wire, we use a steep confinement with $\sigma = 0.1 l_{so}$ and $V_0 = 65 E_{so}$ defined as $V_{conf}(y) = V_{\sigma, V_0}(y - x_0) + V_{\sigma, V_0}(y - L + x_0)$ such that the maxima are located close to the ends of the wire at x_0 and $L - x_0$ where x_0 is chosen such that the

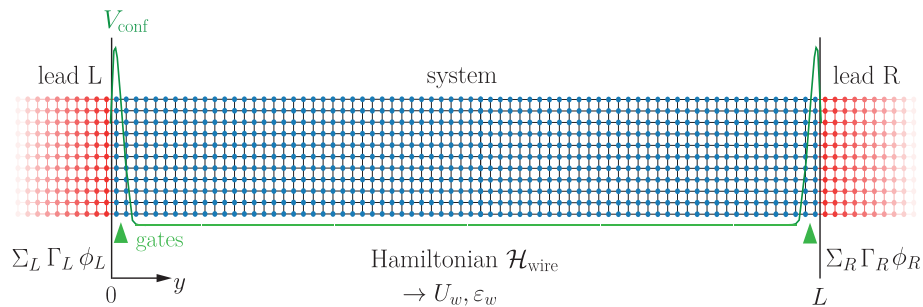


Figure S4. Sketch of the Majorana wire model. We consider leads (red) and wire (blue) of length L to be separated by a confinement potential V_{conf} (green). Using the python package KWANT [1], we define the lattice Hamiltonian, extract the lead self energies Σ_α , Γ_α , propagating modes ϕ_α , and the wire Hamiltonian matrix $\mathcal{H}_{\text{wire}}$ from which we obtain the eigenstates U_w and energy levels ε_w .

potential has decayed to $V_0/2$ at the ends of the wire.

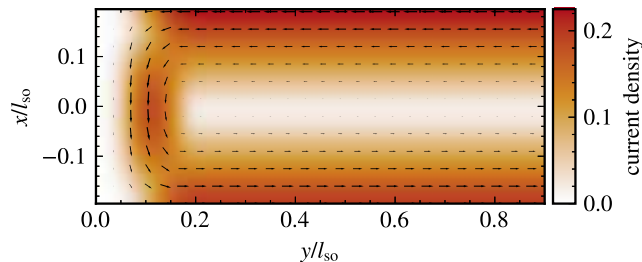


Figure S5. Supercurrent distribution $\mathbf{j}_S \propto \frac{\hbar}{m} \nabla \theta + \frac{2e}{m} \mathbf{A}$ at the left end of the two dimensional wire for the choice of vector potential \mathbf{A} and superconducting order parameter phase θ .

The potential in the leads is given by $V_{\text{lead}} = -100 E_{\text{so}}$ to ensure that both spin components are present at the Fermi level. Leads are modeled with the Hamiltonian

$$\mathcal{H}_{\text{lead}} = \tau_z \left[-\frac{\hbar^2 \partial_y^2}{2m^*} \sigma_0 + V_{\text{lead}} \sigma_0 \right] - E_z \tau_0 \sigma_z . \quad (\text{S4})$$

We consider gates of equal extension that start a distance $0.3 l_{\text{so}}$ from the ends of the wire to not interfere with the confinement potential which is produced by additional gates. Furthermore, we assume that the wire lies a distance $z_{\text{sys}} = 0.3 l_{\text{so}}$ above the gates (see main text Eq. (2)).

D. TWO-DIMENSIONAL WIRE

For the two dimensional case, we additionally choose a wire width $L_x = 0.39 l_{\text{so}}$, chemical potential $\mu = 63 E_{\text{so}}$, Zeeman energy $E_z = 6 E_{\text{so}}$, and otherwise the same parameters as in the one dimensional case. The full 2d Hamiltonian is given by

$$\mathcal{H}_{\text{wire}}^{2d} = \tau_z \left[-\frac{\hbar^2}{2m^*} (\partial_x^2 + \partial_y^2) \sigma_0 - \mu \sigma_0 - i \hbar \alpha_R (\sigma_x \partial_y - \sigma_y \partial_x) + \delta_{\text{dis}}(x, y) \sigma_0 + V_g(x, y) \sigma_0 + V_{\text{conf}}(y) \sigma_0 \right] + \frac{\mu_B g B_z}{2} \tau_0 \sigma_z + \Delta \tau_x \sigma_0 , \quad (\text{S5})$$

with Lande factor $g = -14.9$ [6], and we take into account the orbital effect of the magnetic field by adding a Peierls phase $e^{-ie/\hbar \int_{r_1}^{r_2} \mathbf{A} \cdot d\mathbf{r}}$ to the hoppings. We choose the phase of the superconducting order parameter as $\theta = 0$ and, away from the wire ends, the vector potential as $\mathbf{A} = -B_z x \mathbf{e}_y$, so that it is independent of the coordinate y along

the wire and the energy due to the supercurrent $\mathbf{j}_s = -2en_s(\hbar\nabla\theta + 2e\mathbf{A})/m$ is minimized [7]. At the wire ends we use the following approximation to guarantee current conservation:

$$\mathbf{A} = -a(y)B_z x \mathbf{e}_y + \frac{a'(y)}{2} B_z (x^2 - (L_x/2)^2) \mathbf{e}_x, \quad (\text{S6})$$

$$a(y) = \begin{cases} f_{y_L, y_L + \lambda}(y) & y_L \leq y < y_L + \lambda \\ 1 & y_L + \lambda \leq y \leq y_R - \lambda \\ 1 - f_{x_R - \lambda, x_R}(y) & y_R - \lambda < y \leq y_R \end{cases}, \quad (\text{S7})$$

$$f_{y_1, y_2}(y) = \frac{h(y - y_1)}{h(y - y_1) + h(y_2 - y)} \quad (\text{S8})$$

$$h(y) = \begin{cases} \exp(-\lambda/y) & y > 0 \\ 0 & y \leq 0 \end{cases}, \quad (\text{S9})$$

which ensures that the vector potential at both ends (x_L, x_R) of the wire vanishes over a distance $\lambda = L_x/2$ in a smooth manner. The resulting current \mathbf{j}_s is shown in Fig. S5.

For computing the amplitude during optimization, we take into account the first ten effective energy levels, which speeds up the computations considerably, without influencing the transmission amplitude by a significant amount [5]. We verified this by evaluating the final transmission amplitude after optimization by taking into account 50 levels. In addition, we validated the amplitude in several cases at different steps during the optimization by considering all effective levels for single electron co-tunneling. We find that considering only ten levels during optimization adequately approximates taking the full number of levels into account, as it is relevant for an experiment.

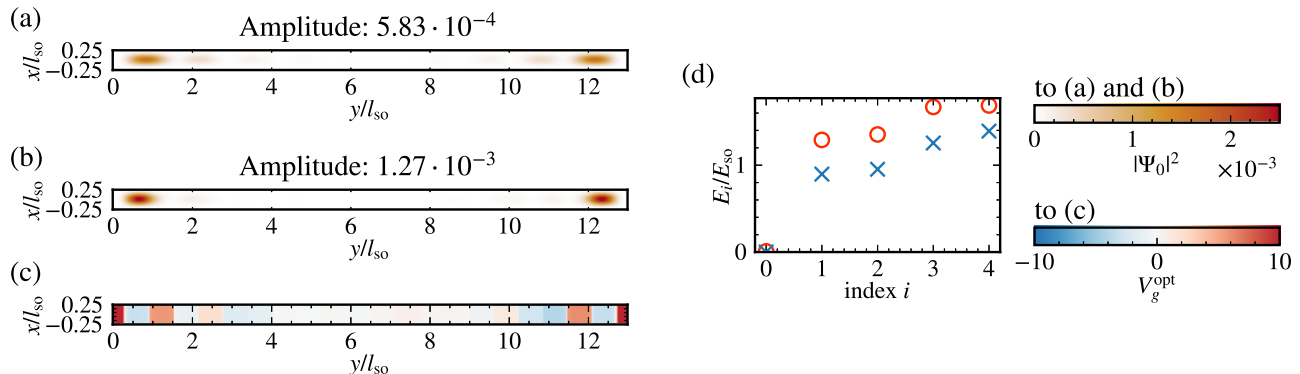


Figure S6. Results for transmission through a two dimensional wire in the topological regime for optimization of the gates. We use 20 gates of equal size along the wire. Wave function $|\Psi_0|^2$ of the lowest level for (a) the reference case without disorder and with zero gate voltage on all gates and (b) optimized gates without disorder (wave function engineering). (c) CMA-ES optimization result for the gate potential that maximizes the transmission amplitude. (d) Energies of the lowest five Bogoliubov levels for the reference case (red circles) and for the optimized gate potential (blue crosses).

E. OPTIMIZATION IN THE SECOND SUBBAND OF THE TWO-DIMENSIONAL WIRE

Gate optimization can also be fruitful for higher subbands, as we show in Fig. S7 where we consider the second topological phase for $\mu = 144.5 E_{so}$, $E_z = 6 E_{so}$, $\Delta = 2 E_{so}$. However, in the presence of levels from different subbands near the Fermi level many subtleties arise that can distract the CMA-ES optimization, such that the optimization is not always able to restore MZMs in presence of disorder. Importantly, different subbands have very different coupling strengths to the leads, e.g. MZMs in the second subband might have smaller couplings than topologically trivial states from the first subband [8]. In order to mitigate this effect, we move both the superconductor and the first/last gate a distance $1.04 l_{so}$ away from the ends of the wire, and add on-site disorder with strength $\delta_{dis} = 100 E_{so}$ to the superconductor-free region [8]. Only moving the superconductor away from the ends and having gates in the normal-conducting regions at the ends would allow the effective chemical potential in the superconductor to change such that the optimization is less stable with the risk of moving completely out of the topological regime. Using

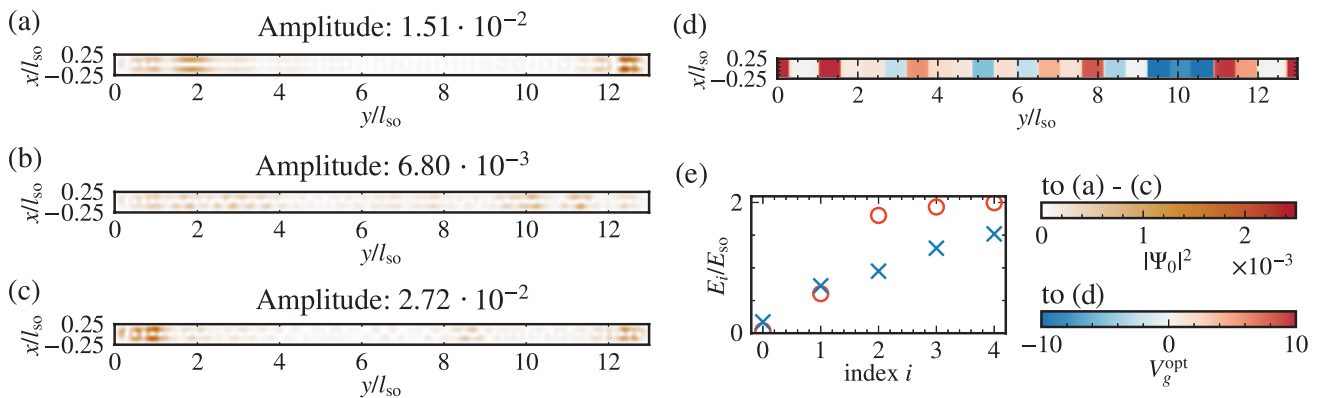


Figure S7. Results for transmission through a two dimensional wire in the topological regime in the second topological phase. Gates and superconductor are moved a distance $1.04 l_{so}$ away from the wire ends and onsite disorder with strength $100 E_{so}$ is added in the normal-conducting region to improve coupling of MZMs to the leads. We use 20 gates of equal size along the wire with $\mu = 244.5 E_{so}$, $E_z = 6 E_{so}$, and $\Delta = 2 E_{so}$. Wave function $|\Psi_0|^2$ of the lowest level for (a) the reference case without disorder and with zero gate voltage on all gates, (b) with bulk disorder ($\lambda_{dis} = 0.052 l_{so}$, $\delta_{dis} = 90 E_{so}$) before gate voltage optimization, and (c) with optimized gate voltages in the presence of disorder. (d) CMA-ES optimization result for the gate potential that maximizes the transmission amplitude. (e) Energies of the lowest five Bogoliubov levels for the reference case (red circles) and for the optimized gate potential (blue crosses).

the modified setup, we find MZMs, which in the reference case without bulk disorder (Fig. S7a) couple about one order of magnitude stronger to the leads than other low energy levels. When adding bulk disorder (Fig. S7b), they are destroyed and low energy levels couple with similar strength to the leads, and after optimization (Fig. S7c), the MZMs are restored with a coupling about twice as strong as other low energy levels. Even with these modifications, in presence of higher subbands at the Fermi level, the occurrence of Andreev bound states and other strongly coupling non-topological low energy states cannot reliably be excluded making the optimization overall more fragile. On the other hand, this also shows that CMA-ES optimization helps with identifying weaknesses in a given setup, such that it can also be used as a tool to test ways to stabilize desired features in the system.

-
- [1] C. W. Groth, M. Wimmer, A. R. Akhmerov, and X. Waintal, Kwant: a software package for quantum transport, *New Journal of Physics* **16**, 063065 (2014).
 - [2] Nikolaus Hansen, yoshihikoueno, ARF1, Kento Nozawa, Matthew Chan, Youhei Akimoto, and Dimo Brockhoff, *CMA-ES/pycma: r3.1.0* (Zenodo, 2021).
 - [3] N. Hansen and A. Ostermeier, Completely derandomized self-adaptation in evolution strategies, *Evolutionary Computation* **9**, 159 (2001).
 - [4] N. Hansen, S. D. Müller, and P. Koumoutsakos, Reducing the time complexity of the derandomized evolution strategy with covariance matrix adaptation (CMA-ES), *Evolutionary Computation* **11**, 1 (2003).
 - [5] M. Thamm and B. Rosenow, Transmission amplitude through a Coulomb blockaded Majorana wire, *Physical Review Research* **3**, 023221 (2021).
 - [6] G. W. Winkler, A. E. Antipov, B. Van Heck, A. A. Soluyanov, L. I. Glazman, M. Wimmer, and R. M. Lutchyn, Unified numerical approach to topological semiconductor-superconductor heterostructures, *Physical Review B* **99**, 245408 (2019).
 - [7] P. Wójcik and M. Nowak, Durability of the superconducting gap in majorana nanowires under orbital effects of a magnetic field, *Physical Review B* **97**, 235445 (2018).
 - [8] F. Pientka, G. Kells, A. Romito, P. W. Brouwer, and F. Von Oppen, Enhanced zero-bias majorana peak in the differential tunneling conductance of disordered multisubband quantum-wire/superconductor junctions, *Physical review letters* **109**, 227006 (2012).